On The Choice of Average Solar Zenith Angle

Timothy W. Cronin *

Program in Atmospheres, Oceans, and Climate, Massachusetts Institute of Technology, Cambridge, Massachusetts

* *Corresponding author address:* MIT, 77 Massachusetts Ave., Cambridge, MA 02139.

E-mail: twcronin@mit.edu

ABSTRACT

Simulations with idealized climate models often choose to neglect spatiotemporal variations in solar radiation, but doing so comes with an important decision about how to average solar radiation in space and time. Since both clear-sky and cloud albedo are increasing functions of the solar zenith angle, one can choose an absorption-weighted zenith angle which reproduces the spatial- or time-mean absorbed solar radiation. Here, we perform calculations for a pure scattering atmosphere and with a more detailed radiative transfer model, and find that the absorption-weighted zenith angle is usually between the daytime-weighted and insolation-weighted zenith angles, but much closer to the insolation-weighted zenith angle in most cases, especially if clouds are responsible for much of the shortwave reflection. Use of daytime-average zenith angle may lead to a high bias in planetary albedo of $\sim$3%, equivalent to a deficit in shortwave absorption of $\sim$10 W m^{-2} in the global energy budget (comparable to the radiative forcing of a roughly sixfold change in CO_2 concentration). Other studies that have used general circulation models with spatially constant insolation have underestimated the global-mean zenith angle, with a consequent low bias in planetary albedo of $\sim$2-6%, or a surplus in shortwave absorption of $\sim$7-20 W m^{-2} in the global energy budget.

1. Introduction

Comprehensive climate models suggest that a global increase in absorbed solar radiation by 1 W m^{-2} would lead to an 0.6-1.1 °C increase in global-mean surface temperatures (*Soden and Held* 2006). The amount of solar radiation absorbed or reflected by the Earth depends on the solar zenith angle (ζ), or angle the sun makes with a line perpendicular to the surface. When the sun is low in the sky (high ζ), much of the incident sunlight may be reflected even for a clear sky; when the sun is high in the sky (low ζ), even thick clouds may not reflect most of the incident sunlight. The difference in average zenith angle between the equator and poles is an important reason why the albedo is typically higher at high latitudes.

In order to simulate the average climate of a planet in radiative-convective equilibrium, one must globally average the incident solar radiation, and define either a solar zenith angle which is constant in time, or which varies diurnally (i.e., the sun rising and setting). The top-of-atmosphere incident solar radiation per unit ground area, or insolation I, is simply the product of the solar constant S_0 and the cosine of the solar zenith angle, $\mu \equiv \cos\zeta$:

$$I = S_0 \cos\zeta, \tag{1}$$

where the planetary-mean insolation is simply $\langle I \rangle = S_0/4 \approx 342$ W m^{-2} (in this paper, we will denote spatial averages with $\langle x \rangle$ and time averages with $\overline{x}$). A global-average radiative transfer calculation requires specifying both an effective cosine of solar zenith angle μ^*, and an effective solar constant, S_0^*, such that the resulting insolation matches the planetary-mean insolation:

$$\langle I \rangle = S_0/4 = S_0^* \mu^*. \tag{2}$$

Matching the mean insolation constrains only the product $S_0^* \mu^*$, and not either parameter individually, so additional assumptions are needed.

The specifics of these additional assumptions are quite important to simulated climate, because radiative transfer processes, most importantly cloud albedo, depend on μ (e.g., *Hartmann* (1994)). For instance, the most straightforward choice for a planetary-average

calculation might seem to be a simple average of μ over the whole planet, including the dark half, so that $S^*_{0S} = S_0$ and μ^*_S=1/4. However, this simple average would correspond to a sun that was always near setting, only ∼15° above the horizon; with such a low sun, the albedo of clouds and the reflection by clear-sky Rayleigh scattering would be highly exaggerated. A more thoughtful, and widely used choice, is to ignore the contribution of the dark half of the planet to the average zenith angle. With this choice of daytime-weighted zenith angle, μ^*_D=1/2, and $S^*_{0D} = S_0/2$.

A slightly more complex option is to calculate the insolation-weighted cosine of the zenith angle, μ^*_I:

$$\mu^*_I = \frac{\int \mu S_0 \mu P(\mu) d\mu}{\int S_0 \mu P(\mu) d\mu}, \tag{3}$$

where $P(\mu)$ is the normalized probability distribution function of global surface area as a function of the cosine of the zenith angle, μ. For the purposes of a planetary average, $P(\mu)$ simply equals 1. This can be seen by rotating coordinates so that the north pole is aligned with the subsolar point, where $\mu = 1$; then μ is given by the sine of the latitude over the illuminated northern hemisphere, and since area is evenly distributed in the sine of the latitude, it follows that area is evenly distributed over all values of μ between 0 and 1. Hereafter, when discussing planetary averages, it should be understood that integrals over μ implicitly contain the probability distribution function $P(\mu) = 1$. Evaluation of (3) gives μ^*_I=2/3, and $S^*_{0I} = 3S_0/8$. Since most of the sunlight falling on the daytime hemisphere occurs where the sun is high, μ^*_I is considerably larger than μ^*_D. A schematic comparison of these three different choices – simple average, daytime-weighted, and insolation-weighted zenith angles – is given in Figure 1.

The daytime-average cosine zenith angle of 0.5 has been widely used. The early studies of radiative-convective equilibrium by *Manabe and Strickler* (1964), *Manabe and Wetherald* (1967), *Ramanathan* (1976), and the early review paper by *Ramanathan and Coakley* (1978), all took $\mu^* = 0.5$. The daytime-average zenith angle has also been used in simulation of climate on other planets (e.g., *Wordsworth et al.* (2010)), as well as estimation of global

radiative forcing by clouds and aerosols (*Fu and Liou* 1993; *Zhang et al.* 2013).

To our knowledge, no studies of global-mean climate with single-column models have used an insolation-weighted cosine zenith angle of 2/3. However, the above considerations regarding spatial averaging over variations in insolation also apply to the temporal averaging of insolation that is required to represent the diurnal cycle, or combined diurnal and annual cycles of insolation, with a zenith angle that is constant in time. In this context, *Hartmann* (1994) strongly argues for the use of insolation-weighted zenith angle, and provides a figure with appropriate daily-mean insolation-weighted zenith angles as a function of latitude for the solstices and the equinoxes (see *Hartmann* (1994), Figure 2.8). *Romps* (2011) also uses an equatorial insolation-weighted zenith in a study of radiative-convective equilibrium with a cloud-resolving model; though other studies that have focused on tropical radiative-convective equilibrium, such as the work by *Tompkins and Craig* (1998), have used a daytime-weighted zenith angle. In large-eddy simulations of marine low clouds, *Bretherton et al.* (2013) advocate for the greater accuracy of the insolation-weighted zenith angle, noting that the use of daytime-weighted zenith angle gives a 20 W m^{-2} stronger negative shortwave cloud radiative effect than the insolation-weighted zenith angle. Biases of such a magnitude would be especially disconcerting for situations where the surface temperature is interactive, as they could lead to dramatic biases in mean temperatures.

Whether averaging in space or time, an objective decision of whether to use daytime-weighted or insolation-weighted zenith angle requires some known and unbiased reference point. In section 2, we develop the idea of absorption-weighted zenith angle as such an unbiased reference point. We show that if albedo depends nearly linearly on the zenith angle, which is true if clouds play a dominant role in solar reflection, then the insolation-weighted zenith angle is likely to be less biased than the daytime-weighted zenith angle. We then calculate the planetary-average absorption-weighted zenith angle for the extremely idealized case of a purely conservative scattering atmosphere. In section 3, we perform calculations with a more detailed shortwave radiative transfer model, and show that differences in plan-

etary albedo between μ_D^*=1/2 and $\mu_I^* = 2/3$ can be ∼3%, equivalent to a radiative forcing difference of over 10 W m^{-2}. In section 4 we show that the superiority of insolation-weighting also applies for diurnally- or annually-averaged insolation. Finally, in section 5, we discuss the implications of our findings for recent studies with global models.

2. Absorption-Weighted Zenith Angle

For the purposes of minimizing biases in solar absorption, the zenith angle should be chosen to most closely match the spatial- or time-mean albedo. By this, we do not intend that the zenith angle should be tuned so as to match the observed albedo over a specific region or time period; rather, we wish to formulate a precise geometric closure on (2). If the albedo is a known function of the zenith angle (i.e., $\alpha = f_\alpha(\mu) = f_\alpha(\cos\zeta)$), then we can choose a zenith angle, μ_A^*, such that its albedo matches the albedo that would be calculated from a full average over space or time (as weighted by the probability density function $P(\mu)$):

$$f_\alpha(\mu_A^*) \int S_0 \mu P(\mu) d\mu = \int S_0 \mu f_\alpha(\mu) P(\mu) d\mu \tag{4}$$

If the albedo function f_α is smooth and monotonic in the zenith angle – the likely (albeit not universal) case for planetary reflection – then f_α can be inverted, and the problem is well-posed, with a unique solution:

$$\mu_A^* = f_\alpha^{-1} \left[\frac{\int \mu f_\alpha(\mu) P(\mu) d\mu}{\int \mu P(\mu) d\mu} \right], \tag{5}$$

where f_α^{-1} represents the inverse function of f_α. Note that for the case of planetary-average climate, $P(\mu) = 1$, and thus (5) simplifies to:

$$\langle \alpha \rangle = 2 \int_0^1 \mu f_\alpha(\mu) d\mu, \tag{6}$$

$$\mu_A^* = f_\alpha^{-1} \left[2 \int_0^1 \mu f_\alpha(\mu) d\mu \right], \tag{7}$$

where $\langle \alpha \rangle$ is the planetary albedo, or ratio of reflected to incident global shortwave radiation. Note that a bias in planetary albedo by 1% would lead to a bias in planetary-average absorbed

shortwave radiation of 3.42 W m^{-2}.

If the albedo is a linear function of the zenith angle, we can write:

$$f_\alpha(\mu) = \alpha_{\max} - \alpha_\Delta \mu, \tag{8}$$

where $\alpha_{\max}$ is the maximum albedo (for $\mu = 0$), and α_Δ is the drop in albedo in going from $\mu = 0$ to $\mu = 1$. In this case, we can show that the absorption-weighted zenith angle is exactly equal to the insolation-weighted zenith angle, regardless of the form of $P(\mu)$. From (3), (4), and (8), it follows that:

$$\begin{aligned} \alpha_{\max} \int \mu P(\mu) d\mu - \alpha_\Delta \mu_A^* \int \mu P(\mu) d\mu &= \alpha_{\max} \int \mu P(\mu) d\mu - \alpha_\Delta \int \mu^2 P(\mu) d\mu \\ \mu_A^* &= \frac{\int \mu^2 P(\mu) d\mu}{\int \mu P(\mu) d\mu} = \mu_I^*. \end{aligned} \tag{9}$$

Thus, if the albedo varies roughly linearly with μ, then we expect the insolation-weighted zenith angle to closely match the absorption-weighted zenith angle.

For planetary-average climate, the simplicity of $P(\mu)$ allows us to perform an additional analytic calculation of the absorption-weighted zenith angle. Consider an albedo similar to (8), but which may now vary nonlinearly, as some power of the cosine of the zenith angle:

$$f_\alpha(\mu) = \alpha_{\max} - \alpha_\Delta \mu^b. \tag{10}$$

The power b is likely equal to or less than 1, so that the albedo is more sensitive to the zenith angle when the sun is low than when the sun is high. For a general value of b, the planetary albedo and absorption-weighted zenith angle are given by:

$$\begin{aligned} \langle \alpha \rangle &= \alpha_{\max} - \frac{\alpha_\Delta}{1 + b/2} \\ \mu_A^* &= \left(\frac{1}{1 + b/2} \right)^{1/b}. \end{aligned} \tag{11}$$

As noted above, if the albedo depends linearly on μ (b=1), then the absorption-weighted zenith angle has a cosine of 2/3, which is equal to to planetary-average value of the insolation-weighted cosine zenith angle (μ_I^*). For $0 < b < 1$, μ_A^* always falls between $e^{-1/2} \approx 0.607$ and

2/3, suggesting that $\mu_I^* = 2/3$ is generally a good choice for the zenith angle in planetary-mean calculations. The albedo must be a strongly nonlinear function of μ, with significant weight at low μ, in order to obtain values of $\mu_A^* < 0.6$.

a. Example: A Pure Scattering Atmosphere

How strongly does the planetary albedo depend on μ for a less idealized function $f_\alpha(\mu)$? For a pure conservative scattering atmosphere, with optical thickness τ^*, two-stream coefficient γ (which we will take =3/4, corresponding to the Eddington approximation (*Pierrehumbert* 2010)), and scattering asymmetry parameter $\hat{g}$, *Pierrehumbert* (2010) (Eqn. 5.38) gives the atmospheric albedo as:

$$\alpha_a = \frac{(1/2 - \gamma\mu)(1 - e^{-\tau^*/\mu}) + (1 - \hat{g})\gamma\tau^*}{1 + (1 - \hat{g})\gamma\tau^*}. \tag{12}$$

Defining a constant surface albedo of α_g, and a diffuse atmospheric albedo α'_a, the total albedo is:

$$\alpha = 1 - \frac{(1 - \alpha_g)(1 - \alpha_a)}{(1 - \alpha_g)\alpha'_a + (1 - \alpha'_a)}. \tag{13}$$

Using this expression, we can calculate how the albedo depends on zenith angle for different sky conditions. Figure 2 shows the dependence of the albedo on the cosine of the solar zenith angle, for a case of Rayleigh scattering by the clear sky ($\tau^* \approx 0.12$, $\hat{g} = 0$), for a cloudy-sky example ($\tau^* = 3.92$, $\hat{g} = 0.843$), and for a linear mix of 68.6 % cloudy and 31.4 % clear sky, which is roughly the observed cloud fraction as measured by satellites (*Rossow and Schiffer* 1999). Values of average cloud optical thickness are taken from *Rossow and Schiffer* (1999), with the optical thickness equal to the sum of cloud and Rayleigh scattering optical thicknesses (3.8 and 0.12, respectively), and the asymmetry parameter set to a weighted average of cloud and Rayleigh scattering asymmetry parameters (0.87 and 0, respectively). Figure 2 also shows the appropriate choice of the cosine of the absorption-weighted zenith angle, μ_A^*, for the clear and cloudy-sky examples. The clear-sky case has $\mu_A^* = 0.55$, the cloudy-sky case has $\mu_A^* = 0.665$, and the mixed-sky case has $\mu_A^* = 0.653$.

We can also use these results to calculate what bias would result from the use of the daytime-weighted zenith angle (μ_D^*=1/2) or the insolation-weighted zenith angle (μ_I^*=2/3). The planetary albedo is generally overestimated by use of μ_D^* and underestimated by use of μ_I^*; the first three rows of Table 1 summarize our findings for a pure scattering atmosphere. For a clear sky, the daytime-weighted zenith angle is a slightly more accurate choice than the insolation-weighted zenith angle. On the other hand, for a cloudy sky with moderate optical thickness, the insolation-weighted zenith angle is essentially exact, and a daytime-weighted zenith angle may overestimate the planetary albedo by over 7%. For Earthlike conditions, with a mixed sky that has low optical thickness in clear regions, and moderate optical thickness in cloudy regions, a cosine-zenith angle close to but slightly less than the planetary insolation-weighted mean value of 2/3 is likely the best choice. The common choice of μ^*=1/2 will overestimate the negative shortwave radiative effect of clouds, while choices of μ^* that are larger than 2/3 will underestimate the negative shortwave radiative effect of clouds. Our calculations here, however, are quite simplistic, and do not account for atmospheric absorption or wavelength-dependent optical properties. In the following section, we will use a more detailed model to support the assertion that the insolation-weighted zenith angle leads to smaller albedo biases than the daytime-weighted zenith angle.

3. Calculations with a Full Radiative Transfer Model

The above calculations provide a sense for the magnitude of planetary albedo bias that may result from different choices of average solar zenith angle. In this section, we calculate albedos using version 3.8 of the shortwave portion of the Rapid Radiative Transfer Model, for application to GCMs (RRTMG_SW, v3.8; *Iacono et al.* (2008); *Clough et al.* (2005)); hereafter we refer to this model as simply "RRTM" for brevity. Calculations with RRTM allow for estimation of biases associated with different choices of μ when the atmosphere has more realistic scattering and absorption properties than we assumed in the pure scattering

expressions above (12), (13). RRTM is a broadband, two-stream, correlated k-distribution radiative transfer model, which has been tested against line-by-line radiative transfer models, and is used in several general circulation models (GCMs). For calculation of radiative fluxes in partly cloudy skies, the model uses the Monte-Carlo independent column approximation (McICA; *Pincus et al.* (2003)), which stochastically samples 200 profiles over the prescribed range of combinations of cloud fraction at different vertical levels, and averages the fluxes that result.

We use RRTM to calculate the albedo as a function of zenith angle for a set of built-in reference atmospheric profiles, and several cloud profile assumptions. The atmospheric profiles we use are the Tropical atmosphere, the 1976 U.S. Standard Atmosphere, and the Subarctic Winter atmosphere, and we perform calculations with clear skies, as well as two cloud profile assumptions (Table 2). One cloud profile is a mixed sky, intended to mirror Earth's climatological cloud distribution, with four cloud layers having fractional coverage, water path, and altitudes based *Rossow and Schiffer* (1999); we call this case "RS99". The other cloud profile is simply fully overcast with a low-level "Stratocumulus" cloud deck, having a water path of 100 g/m^2. Table 2 gives the values for assumed cloud fractions, altitudes, and in-cloud average liquid and ice water in clouds at each level. Cloud fractions have been modified from Table 4 of *Rossow and Schiffer* (1999) because satellites see clouds from above, and will underestimate true low cloud fraction that is overlain by higher clouds. If multiple cloud layers are randomly overlapping, and seen from above, then, indexing cloud layers as (1,2,...) from the top down, we denote $\hat{\sigma}_i$ as the observed cloud fraction in layer i, and σ_i as the true cloud fraction in layer i. Then the true cloud fraction in layer i is:

$$\sigma_i = \hat{\sigma}_i \left(1 - \sum_{j=1}^{i-1} \hat{\sigma}_j \right)^{-1}, \tag{14}$$

which can be seen because the summation gives the fraction of observed cloudy sky above level i, so the term in parentheses gives the fraction of clear sky above level i, which is equal to the ratio of observed cloud fraction to true cloud fraction in layer i (again assuming random

cloud overlap). Applying this correction to observed cloud fractions $(\hat{\sigma_1}, \hat{\sigma_2}, \hat{\sigma_3}, \hat{\sigma_4})$=(0.196, 0.026, 0.190, 0.275) from Table 4 of *Rossow and Schiffer* (1999) gives the cloud fractions listed in Table 2: $(\sigma_1, \sigma_2, \sigma_3, \sigma_4)$=(0.196, 0.032, 0.244, 0.467).

To isolate the contributions from changing atmospheric (and especially cloud) albedo as a function of μ, the surface albedo is set to a value of 0.12 for all calculations, independent of the solar zenith angle. The surface albedo value of 0.12 is chosen following the observed global mean surface reflectance from Figure 5 of *Donohoe and Battisti* (2011) (average of the hemispheric values from observations). Using RRTM calculations of albedo at 22 roughly evenly-spaced values of μ, we interpolate $f_\alpha(\mu)$ to a grid in μ with spacing 0.001, calculate the planetary albedo $\langle\alpha\rangle$ from equation (6), and find the value of μ_A^* whose albedo most closely matches $\langle\alpha\rangle$. The dependence of albedo on μ is shown in Figure 3; atmospheric absorption results in generally lower values of albedo than in the pure scattering cases above, as well as lower sensitivity of the albedo to zenith angle. For partly or fully cloudy skies, the albedo is approximately linear in the zenith angle. Note that $f_\alpha(\mu)$ here is not necessarily monotonic, as it decreases for very small μ. This implies that the inverse problem can return two solutions for μ_A^* in some cases; we select the larger result if this occurs.

For clear skies, biases in $\langle\alpha\rangle$ are nearly equal in magnitude for μ_D^* and μ_I^* (Table 1). For partly cloudy or overcast skies, however, biases in $\langle\alpha\rangle$ are much larger for μ_D^* than for μ_I^*; the insolation-weighted zenith angle has an albedo bias that is lower by an order of magnitude than the albedo bias of the daytime-weighted zenith angle. The bias in solar absorption for partly-cloudy or overcast skies for μ_D^* is on the order of 10 W m^{-2}. While we have only tabulated biases for the 1976 U.S. Standard Atmosphere, results are similar across reference atmospheric profiles.

4. Diurnal and Annual Averaging

Thus far, we have presented examples of albedo biases only for the case of planetary-mean calculations. The absorption-weighted zenith angle can also be calculated and compared to daytime-weighted and insolation-weighted zenith angles for the case of diurnal- or annual-average solar radiation at a single point on the Earth's surface, using (5). The latitude and temporal averaging period both enter into the calculation of the probability density function $P(\mu)$, as well as the bounds of the integrals in (5). We will look at how μ_A^* varies as a function of latitude for two cases: an equinoctial diurnal cycle and a full average over annual and diurnal cycles. In both cases, we will use $f_\alpha(\mu)$ as calculated by RRTM, for the 1976 U.S. Standard Atmosphere, and the mixed-sky cloud profile of RS99.

For an equinoctial diurnal cycle at latitude ϕ, the cosine of the zenith angle is given by $\mu(h) = \cos\phi\cos(\pi(h-12)/12)$, where h is the local solar time in hours. Since time (h) is uniformly distributed, this can be analytically transformed to obtain the probability density function $P(\mu)$:

$$P(\mu) = \frac{2}{\pi\sqrt{\cos^2\phi - \mu^2}}, \tag{15}$$

which is valid for $0 \leq \mu < \cos\phi$. For the equinoctial diurnal cycle, daytime-weighting gives $\mu_D^* = (2/\pi)\cos\phi$, while insolation-weighting gives $\mu_I^* = (\pi/4)\cos\phi$. Figure 4 shows that the absorption-weighted zenith angle is once again much closer to the insolation-weighted zenith angle than to the daytime-weighted zenith angle for partly cloudy skies. We can also look at how the time-mean albedo $\overline{\alpha}$ compares to the albedo calculated from μ_D^* or μ_I^*. Albedo biases at the equator are -0.2% for insolation-weighting, and +2.6% for daytime-weighting, which translates to solar absorption biases of +0.9 W m^{-2} and -11.2 W m^{-2}, respectively. For clear-sky calculations (not shown), results are also similar to what we found for planetary-average calculations: the two choices are almost equally biased, with albedo underestimated by $\sim$0.5% when using μ_I^*, and overestimated by $\sim$0.5% when using μ_D^*.

For the full annual and diurnal cycles of solar insolation, $P(\mu)$ must be numerically tab-

ulated. For each latitude band, we calculate μ every minute over a year, and construct $P(\mu)$ histograms with bin width 0.001 in μ; then we calculate the insolation-weighted, daytime-weighted, and absorption weighted cosine zenith angles and corresponding albedos (Figure 5). For partly cloudy skies, the insolation-weighted zenith angle is a good match to the absorption-weighted zenith angle, with biases in albedo of less than 0.2%. Albedo biases for the daytime-weighted zenith angle are generally $\sim$2-3%, with a maximum of over 3% around 60 degrees latitude. The solar absorption biases at the equator are similar to those found in the equinoctial diurnal average, though slightly smaller. Overall, these findings indicate that insolation-weighting is generally a better approach than daytime-weighting for representing annual or diurnal variations in solar insolation.

5. Discussion

The work presented here addresses potential climate biases in two major lines of inquiry in climate science. One is the use of single-column models in radiative-convective equilibrium as a tool to simulate and understand important aspects of planetary-mean climate, such as surface temperature and precipitation. The second is the increasing use of idealized three-dimensional general circulation models (GCMs) for understanding large-scale atmospheric dynamics. Both of these categories span a broad range of topics, from understanding the limits of the circumstellar habitable zone and the scaling of global-mean precipitation with temperature in the case of single-column models, to the location of midlatitude storm tracks and the strength of the Hadley circulation in the case of idealized GCMs. Both categories of model often sensibly choose to ignore diurnal and annual variations in solar insolation, so as to reduce simulation times and avoid unnecessary complexity. Our work suggests that spatial or temporal averaging of solar radiation, however, can lead to biases in total absorbed solar radiation on the order of 10 W m^{-2}, especially if the models used have a large cloud area fraction.

Single column models are a valuable tool for understanding the controls on global-mean surface temperature, and its sensitivity to forcing by changes in solar radiation or greenhouse gases. The extent to which a single-column model with unbiased planetary albedo and relative humidity, accurately captures the global-mean surface temperature of both the real Earth, and more complex three-dimensional GCMs, is a key test of the magnitude of nonlinearities in the climate system. For instance, variability in tropospheric relative humidity, as induced by large-scale vertical motions in the tropics, can give rise to dry-atmosphere "radiator fin" regions that emit longwave radiation to space more effectively than would a horizontally uniform atmosphere, resulting in a cooling of global mean temperatures relative to a reference atmosphere with homogeneous relative humidity (*Pierrehumbert* 1995). The relative and absolute importance of nonlinearities such as these subtropical "radiator fins," or impacts of ice on planetary albedo, or interactions between clouds and large-scale dynamics, or spatiotemporal variability in lapse rates, represents a fundamental and unanswered question in climate science, in part because single-column models have generally been tuned in ways that makes unbiased comparison of their absolute temperature with global models difficult.

The recent work of *Popke et al.* (2013) elegantly seeks to bridge this gap, by using a global model (ECHAM6) with uniform insolation, and no rotation. They thus simulate planetary radiative-convective equilibrium over a slab ocean, allowing for organization of convection and circulations up to planetary scales. One of their findings that deserves more explanation is that their planetary albedo is $\sim$0.2, much lower than the observed value of 0.3 (e.g., *Hartmann* (1994)), and surface temperatures are $\sim$28 °C, substantially warmer than the observed surface temperatures of $\sim$14 °C. The warm temperatures and nonrotating dynamics spur comparison of their simulated cloud and relative humidity distributions to the Earth's Tropics, but the basic question of why albedo is so low, and temperatures so warm, goes largely unanswered. While part of the answer is likely their low value of surface albedo (0.07), our work also suggests that their use of a uniform equatorial equinox diurnal cycle,

with $\mu_I^* = \pi/4$, may underestimate cloud and clear-sky albedo. For RS99 clouds and an equatorial equinox diurnal cycle, we estimate a time-mean albedo of 32.7%; the same cloud field would give a planetary albedo of 34.6% if the planetary-average insolation-weighted cosine zenith angle of 2/3 were used. Thus, we estimate that the shortwave absorption in *Popke et al.* (2013) may be biased by $\sim$6.7 W m^{-2}.

Previous simulations by *Kirtman and Schneider* (2000), and *Barsugli et al.* (2005) also found very warm global-mean temperatures when insolation contrasts were removed, though planetary rotation was retained in both studies. *Kirtman and Schneider* (2000) found a global-mean surface temperature of 26 °C with a reduced global-mean insolation of only 315 W m^{-2}; realistic global-mean insolation led to too-warm temperatures and numerical instability. *Kirtman and Schneider* (2000) offer little explanation for the extreme warmth of their simulations, but apparently also chose to homogenize radiation by using an equatorial equinox diurnal cycle, with $\mu_I^* = \pi/4$. *Barsugli et al.* (2005) obtained a global-mean surface temperature of $\sim$38 °C when using a realistic global-mean insolation of 340 W m^{-2}. Similarly to *Popke et al.* (2013), *Barsugli et al.* (2005) also invoke a low planetary albedo of 0.21 as a plausible reason for their global warmth, and explain their low albedo as a consequence of a dark all-ocean surface. This work, however, suggests that their unphysical use of constant $\mu = 1$ may lead to a large albedo bias on its own. For RS99 clouds, we estimate an albedo of 28.8% for μ=1, as compared to 34.6% for μ=2/3, so their albedo bias may be as large as -5.8%, with a resulting shortwave absorption bias of +19.8 W m^{-2}. Application of these three studies (*Kirtman and Schneider* 2000; *Barsugli et al.* 2005; *Popke et al.* 2013) to ask questions about the importance of climate nonlinearities may thus be impeded by biases in planetary albedo and temperature due to a sun that is too high in the sky. While it was not the primary focus of these studies to query the importance of climate nonlinearities, these studies nonetheless serve as a reminder that care is required when using idealized solar geometry in models.

Our work here has focused on matching the top-of-atmosphere absorbed shortwave ra-

diation, but this does not guarantee unbiased partitioning into atmospheric and surface absorption. Because global-mean temperatures are quite sensitive to planetary albedo, we have focused in this work on matching the top-of-atmosphere shortwave absorption, but our methods could easily be extended to match some other quantity instead, such as the shortwave radiation absorbed by the surface. Based on our calculations with RRTM, it appears that a single value of $\mu \sim 0.58$ will give both the correct planetary albedo and the correct partitioning of absorbed shortwave radiation for clear skies; however, for partly cloudy or overcast skies, a single value of μ cannot simultaneously match both the planetary albedo and the partitioning of absorbed shortwave radiation. Together with the correspondence between global precipitation and free-tropospheric radiative cooling (e.g., *Takahashi* (2009)), the dependence of atmospheric solar absorption on zenith angle suggests that idealized simulations could obtain different relationships between temperature and precipitation due solely to differences in solar zenith angle.

Finally, we note that the use of an appropriately-averaged solar zenith angle still has obvious limitations. Any choice of insolation that is constant in time cannot hope to capture any covariance between albedo and insolation, which might exist due to diurnal or annual cycles of cloud fraction, height, or optical thickness. Furthermore, use of an absorption-weighted zenith angle will do nothing to remedy model biases in cloud fraction or water content that arise from the model's convection or cloud parameterizations. We hope that the methodology and results introduced in this paper will mean that future studies make better choices with regards to solar zenith angle averaging, and thus will not convolute real biases in cloud properties with artificial biases in cloud radiative effects that are solely related to zenith angle averaging.

Acknowledgments.

Thanks to Kerry Emanuel, Martin Singh, Aaron Donohoe, and Peter Molnar for useful conversations. This work was funded by NSF Grant 1136480, The Effect of Near-Equatorial

Islands on Climate.

REFERENCES

Barsugli, J., S. Shin, and P. Sardeshmukh, 2005: Tropical Climate Regimes and Global Climate Sensitivity in a Simple Setting. *J. Atmos. Sci.*, **62**, 1226–1240.

Bretherton, C., P. Blossey, and C. Jones, 2013: Mechanisms of marine low cloud sensitivity to idealized climate perturbations: A single-LES exploration extending the CGILS cases. *J. Adv. Model. Earth Sys.*, **5**, 316–337, doi:10.1002/jame.20019.

Clough, S., M. Shephard, E. Mlawer, J. Delamere, M. Iacono, K. Cady-Pereira, S. Boukabara, and P. Brown, 2005: Atmospheric radiative transfer modeling: a summary of the AER codes. *J. Quant. Spectrosc. Radiat. Transfer*, **91**, 233–244.

Donohoe, A., and D. Battisti, 2011: Atmospheric and Surface Contributions to Planetary Albedo. *J. Climate*, **24**, 4402–4418, doi:10.1175/2011JCLI3946.1.

Fu, Q., and K. Liou, 1993: Parameterization of the Radiative Properties of Cirrus Clouds. *J. Atmos. Sci.*, **50**, 2008–2025.

Hartmann, D., 1994: *Global Physical Climatology*. Academic Press, International Geophysics Series Volume 56, San Diego, 409 pp.

Iacono, M., J. Delamere, E. Mlawer, M. Shephard, S. Clough, and W. Collins, 2008: Radiative forcing by long-lived greenhouse gases: Calculations with the AER radiative transfer models. *J. Geophys. Res.*, **113**, D13103, doi:10.1029/2008JD009944.

Kirtman, B., and E. Schneider, 2000: A Spontaneously Generated Tropical Atmospheric General Circulation. *J. Atmos. Sci.*, **57**, 2080–2093.

Manabe, S., and R. Strickler, 1964: Thermal equilibrium of the atmosphere with a convective adjustment. *J. Atmos. Sci.*, **21**, 361–385.

Manabe, S., and R. Wetherald, 1967: Thermal equilibrium of the atmosphere with a given distribution of relative humidity. *J. Atmos. Sci.*, **24**, 241–259.

Pierrehumbert, R., 1995: Thermostats, Radiator Fins, and the Local Runaway Greenhouse. *J. Atmos. Sci.*, **52**, 1784–1806.

Pierrehumbert, R., 2010: *Principles of Planetary Climate*. Cambridge University Press, Cambridge, UK, 652 pp.

Pincus, R., H. Barker, and J. Morcrette, 2003: A fast, flexible, approximation technique for computing radiative transfer in inhomogeneous cloud fields. *J. Geophys. Res.*, **108**(D13), 4376, doi:10.1029/2002JD003322.

Popke, D., B. Stevens, and A. Voigt, 2013: Climate and Climate Change in a Radiative-Convective Equilibrium Version of ECHAM6. J. Adv. Model. Earth Sys., **5**, 1–14, doi:10.1029/2012MS000191.

Ramanathan, V., 1976: Radiative Transfer Within the Earth's Troposphere and Stratosphere: A Simplified Radiative-Convective Model. *J. Atmos. Sci.*, **33**, 1330–1346.

Ramanathan, V., and J. Coakley, 1978: Climate Modeling Through Radiative-Convective Models. *Reviews of Geophysics and Space Physics*, **16**, 465–489.

Romps, D., 2011: Response of Tropical Precipitation to Global Warming. *J. Atmos. Sci.*, **68**, 123–138, doi:10.1175/2010JAS3542.1.

Rossow, W., and R. Schiffer, 1999: Advances in Understanding Clouds from ISCCP. *Bull. Amer. Meteor. Soc.*, **80**, 2261–2287.

Soden, B., and I. Held, 2006: An assessment of climate feedbacks in coupled ocean-atmosphere models. *J. Climate*, **19**, 3354-3360, doi:10.1175/JCLI3799.1.

Takahashi, K., 2009: Radiative constraints on the hydrological cycle in an idealized radiative-convective equilibrium model. *J. Atmos. Sci.*, **66**, 77–91, doi:10.1175/2008JAS2797.1.

406 Tompkins, A., and G. Craig, 1998: Radiative-convective equilibrium in a three-dimensional
407 cloud-ensemble model. *Quart. J. Roy. Meteor. Soc.*, **124**, 2073–2097.

408 Wordsworth, R., F. Forget, F. Selsis, J. Madeleine, E. Millour, and V. Eymet, 2010: Is Gliese
409 581d habitable? Some constraints from radiative-convective climate modeling. *Astron.*
410 *Astrophys.*, **522**, A22, doi: 10.1051/0004-6361/201015053.

411 Zhang, L., Q. Li, Y. Gu, K. Liou, and B. Meland, 2013: Dust vertical profile impact on
412 global radiative forcing estimation using a coupled chemical-transport-radiative-transfer
413 model. *Atmos. Chem. Phys.*, **13**, 7097–7114, doi:10.5194/acp-13-7097-2013.

List of Tables

TABLE 1. Table of planetary albedos and biases.

Radiative Transfer Model	Atmospheric Profile	$\langle\alpha\rangle$ (%)	μ_A^*	Biases in α (%) μ=1/2	μ=2/3
Pure scattering	clear sky	19.9	0.550	0.78	-1.40
Pure scattering	68.6% ISCCP cloud, 31.4% clear	31.9	0.653	5.57	-0.49
Pure scattering	ISCCP cloud	37.4	0.665	7.77	-0.08
RRTM	1976 U.S. Standard - clear	14.1	0.576	0.56	-0.53
RRTM	1976 U.S. Standard - RS99 clouds	34.8	0.657	3.16	-0.19
RRTM	1976 U.S. Standard - Stratocumulus	51.5	0.686	3.53	0.37

TABLE 2. Cloud profiles used in calculations with RRTM. The multiple cloud layers of *Rossow and Schiffer* (1999) are used together, and are assumed to overlap randomly. Cloud fractions are based on Table 4 of *Rossow and Schiffer* (1999), but adjusted for random overlap and observation from above (see text). Cloud-top altitudes are based on top pressures from *Rossow and Schiffer* (1999) and pressure-height profile from 1976 U.S. Standard Atmosphere. Cloud water/ice allocation uses 260 K as a threshold temperature.

Cloud Profile	fraction (-)	top altitude (km)	water path (g/m^2)	ice path (g/m^2)
Rossow and Schiffer (1999) RS99 low	0.475	2	51	0
Rossow and Schiffer (1999) RS99 medium	0.244	5	0	60
Rossow and Schiffer (1999) RS99 convective	0.032	9	0	261
Rossow and Schiffer (1999) RS99 cirrus	0.196	10.5	0	23
Stratocumulus	1.0	2	100	0

List of Figures

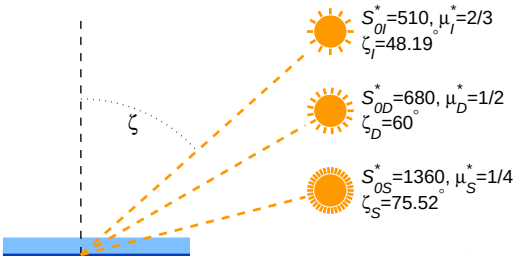

FIG. 1. Schematic example of three different choices of zenith angle and solar constant that give the same insolation. The solar zenith angle ζ is shown for each of the three choices, which correspond to simple average, daytime-weighted, and insolation-weighted choices of μ, as in the text.

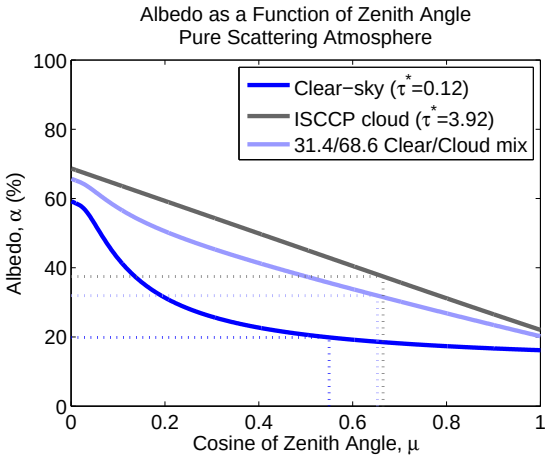

FIG. 2. Plot of albedo against cosine of the zenith angle, for a pure conservative scattering atmospheric column, based on *Pierrehumbert* (2010), Eqn. (5.41). We show calculations for a clear-sky case with τ^*=0.12 and $\hat{g}$=0 (blue), for a cloudy case, with τ^*=3.92 and $\hat{g}$=0.843 (gray), and a linear mix of the two for a sky that is 68.6 % cloudy and 31.4 % clear (blue-gray). The average cloud fraction and optical thickness are taken after International Satellite Cloud Climatology Project (ISCCP) measurements (*Rossow and Schiffer* 1999), and the surface albedo is set to a constant of 0.12, independent of μ. The values of the cosines of absorption-weighted zenith angle are indicated by the x-locations of the vertical dotted lines, and the planetary average albedos are indicated by the y-locations of the horizontal dotted lines (see also Table 1).

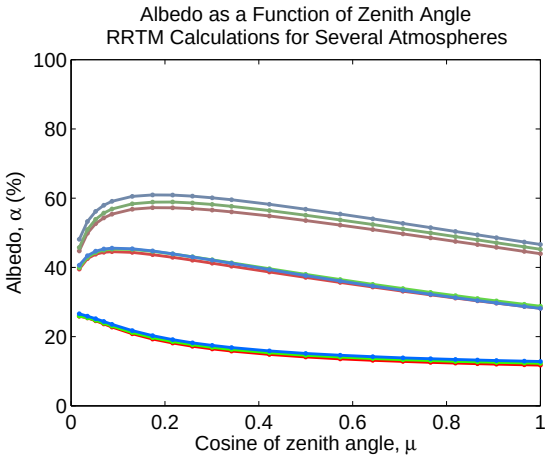

FIG. 3. Plot of albedo against cosine of the zenith angle, for calculations from RRTM. Albedo is shown for three atmospheric profiles: Tropical (red), 1976 U.S. Standard (green), and Subarctic winter (blue). We also show results for clear-sky radiative transfer (bottom set of lines), as well two cloud profile assumptions: observed RS99 cloud climatology (middle set of lines), and Stratocumulus overcast (upper set of lines) – see Table 2 for more details on cloud assumptions. The surface albedo is set to a constant of 0.12 in all cases, independent of μ.

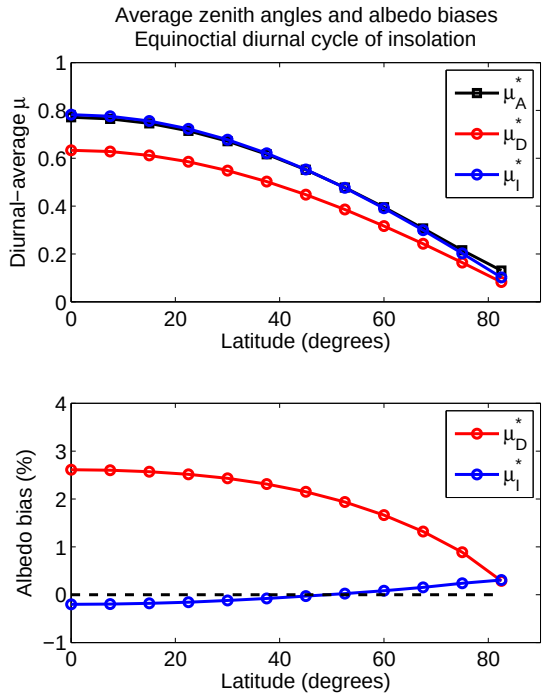

FIG. 4. Plot of diurnal-average zenith angles (top), and biases in time-mean albedo (bottom) for equinoctial diurnal cycles, as a function of latitude. Albedo is calculated in RRTM, using the 1976 U.S. Standard Atmosphere and RS99 clouds (Table 2). Albedo biases for the daytime-weighted zenith angle (μ_D^*, red) and the insolation-weighted zenith angle (μ_I^*, blue) are calculated relative to the absorption-weighted zenith angle (μ_A^*, black).

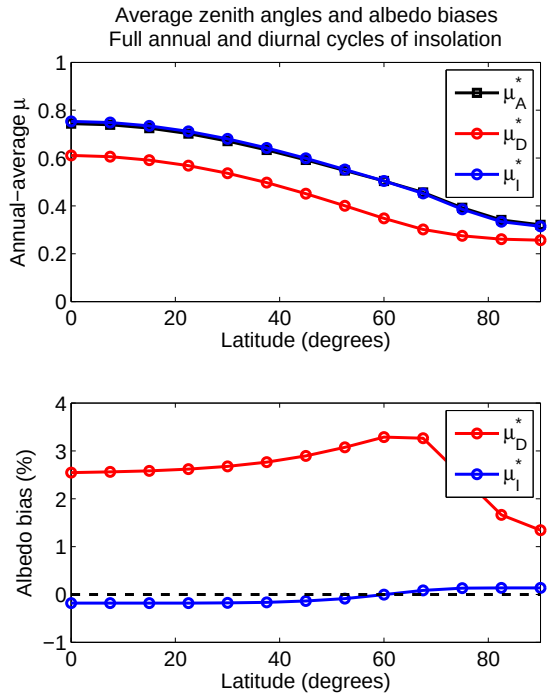

FIG. 5. Plot of annual-average zenith angles (top), and biases in time-mean albedo (bottom) for full annual and diurnal cycles of solar insolation, as a function of latitude. Albedo is calculated in RRTM, using the 1976 U.S. Standard Atmosphere and RS99 clouds (Table 2). Albedo biases for the daytime-weighted zenith angle (μ_D^*, red) and the insolation-weighted zenith angle (μ_I^*, blue) are calculated relative to the absorption-weighted zenith angle (μ_A^*, black).